Thermal expansion behavior of sintered Nd–Fe–B magnets with different Co contents and orientations

Rui-Yang Meng(孟睿阳), Ji-Yuan Xu(徐吉元), Jia-Teng Zhang(张家滕), Jing Liu(刘静), Yi-Kun Fang(方以坤), Sheng-Zhi Dong(董生智)†, and Wei Li(李卫)

Division of Functional Material, Central Iron & Steel Research Institute, Beijing 100081, *China*

(Received 22 November 2022; revised manuscript received 3 March 2023; accepted manuscript online 31 March 2023)

The thermal expansion behavior of sintered Nd–Fe–B magnets is a crucial parameter for production and application. However, this aspect has not been thoroughly investigated. In this study, three different sintered Nd–Fe–B magnets with varying Co content (Co = 0, 6, 12 wt%) were prepared using the conventional powder metallurgy method, and four magnets oriented under different magnetic fields were prepared to compare. The thermal expansion behavior for the magnets was investigated using a linear thermal dilatometry in the temperature range of 20 °C–500 °C. It was found that, the coefficient of thermal expansion (CTE) increases with the increase of Co contents, while the anisotropy of thermal expansion decreases. The introduction of Co leads to continuous changes from negative to positive thermal expansion in the vertically oriented direction, which is important for the development of zero thermal expansion magnets. The thermal expansion of non-oriented magnets was found to be isotropic. Additionally, the anisotropy of thermal expansion increases with the increase of orientation degree. These results have important implications for the development of sintered Nd–Fe–B with controllable CTE.

Keywords: thermal expansion, sintered Nd–Fe–B magnets, orientation, Co content

PACS: 65.40.De, 75.50.Ww, 61.30.Gd, 77.80.bg **DOI:** 10.1088/1674-1056/acc933

1. Introduction

Sintered Nd–Fe–B magnets (S-NdFeB) have become the most widely used rare-earth permanent magnets (REPMs) today due to their superior magnetic properties and cost performance, and play an important role in various fields such as new energy vehicles, wind power generators, and electronic devices.[1–4]

The thermal expansion behavior is a crucial metric for evaluating the ability of REPMs to maintain stability under complex working conditions. However, compared to conventional alloys, S-NdFeB exhibits unusual anisotropically anomalous in thermal expansion. Specifically, in the temperature range of 20 °C–100 °C, the linear coefficient of thermal expansion (CTE, α_l) for S-NdFeB is $\alpha_l^{\perp} = -2\times10^{-6}$ K^{-1} $\sim$ 0×10^{-6} K^{-1} (in the direction perpendicular to orientation, $\perp$, negative thermal expansion, NTE) and $\alpha_l^{\parallel} = 4\times10^{-6}$ K^{-1} $\sim$ 9×10^{-6} K^{-1} (in the direction parallel to orientation, $\parallel$, positive thermal expansion, PTE).[5] In contrast, for most soft magnetic alloys, α_l is isotropic and falls within the in the range of 6.81×10^{-6} K^{-1} $\sim$ 13.3×10^{-6} K^{-1}.[6–10] The discrepancy in CTE between S-NdFeB and soft magnetic alloys may result in detachment or compression during their assembly, significantly impacting the system's stability. Similarly, this discrepancy challenges to the welding of S-NdFeB with the latter.[11] In addition, CTE plays a crucial role in the production and preparation of REPM. Sun found that the anisotropic CTE leads to $SmCo_5$ ring magnets, and calculated out the critical orientation degree of fracture.[12] Similarly, Ishimoto studied the fracture mechanism of radially oriented Nd–Fe–B ring magnets and attributed cracking to accumulated thermal stress resulting from the anisotropic CTE of the oriented sintered magnets during cooling.[13] Anisotropic anomalous thermal expansion in the lattices of $R_2Fe_{14}B$ compounds has been reported in several studies,[14–18] with the joint action of the Fe sublattice and the R sublattice causing spontaneous magnetostriction, which is a major factor in anomalous thermal expansion.[14] Andreev studied the lattice thermal expansion of $Y_2(Fe_{1-x}Co_x)_{14}B$ ($x = 0$, 0.1, 0.2, and 0.3) compounds and found that the Invar-type anomaly decreases with increasing of Co substitution.[19] Recent study on $Er_2(Fe_{1-x}Co_x)_{14}B$ ($x = 0$, 0.05, and 0.1) compounds have revealed similar phenomena.[20]

Most research on anomalous thermal expansion and spontaneous magnetostriction has focused on the single-phase $R_2Fe_{14}B$-type compound samples. However, the thermal expansion behavior of S-NdFeB with complex phase structure is more valuable to research for practical application. The primary objective of this study is to investigate the thermal expansion behavior of S-NdFeB and develop a method for regulation. In this paper, three different S-NdFeB magnets with varying Co content (Co = 0, 6, 12 wt%) were prepared using the conventional powder metallurgy method, and four magnets

†Corresponding author. E-mail: dong_shengzhi@163.com

© 2023 Chinese Physical Society and IOP Publishing Ltd

oriented under different magnetic field were prepared to compare. We analyzed the thermal expansion characteristics of the magnets in terms of Co content and orientation, yielding important insights into the development of sintered NdFeB with elevated thermal stability.

2. Experimental details

Alloys with the compositions of

$$(\mathrm{Pr,Nd,Dy})_{31.2}\mathrm{Co}_x\mathrm{Fe}_{\mathrm{bal}}\mathrm{B}_{1.0}M_{0.6}$$
$$(M=\mathrm{Cu,Al,Zr})\ \ (x=0,6,12\ \mathrm{wt\%})$$

were prepared in the form of flakes about 0.3-mm thick using strip casting technique. After hydrogen decrepitation (HD), the alloys were subjected to jet milling (JM) in nitrogen to obtain powders with the average particle size about 2.7 μm–2.9 μm (surface mean diameter). The obtained powders were compacted and aligned under a magnetic field of 2 T and followed by isostatic pressing under a pressure of 200 MPa. Green compacts were sintered in a vacuum at 1050 °C–1070 °C for 3 h and additionally annealed at 880 °C–900 °C for 2 h subsequently at 480 °C–500 °C for 3 h. According to the Co content x, the corresponding magnets were defined as Co0, Co6, and Co12. Another alloy of $(\mathrm{Pr,Nd,Dy})_{32.2}\mathrm{Co}_{5.8}\mathrm{Fe}_{\mathrm{bal}}\mathrm{B}_{1.0}M_{0.6}$ (M = Cu, Al, Zr) were used to prepare the magnets with different easy-axis orientations. The powders were compacted and aligned under a magnetic field producing by the current of 0 A, 30 A, 60 A, and 90 A, respectively (the measured magnetic fields correspond to 0 T, 0.63 T, 1.64 T, and 1.94 T). The rest of processes was same as above. According to the current, the magnets with different orientation degrees are defined as 0 A, 30 A, 60 A, 90 A.

The magnetic properties measurement at different temperatures were carried out using a permanent magnetic measurement system (NIM-6500C, China). To represent the phase composition and orientation degree, x-ray diffraction (XRD, Rigaku Smartlab, Japan) was used. Electron backscatter diffraction (EBSD, JSM7200F with EDAX assembly, Japan) was used to further characterize the degree of orientation. The linear thermal expansion measurement in the range of 20 °C–500 °C were carried out using a thermal dilatometer (DIL, Netzsch DIL 402 Expedis Supreme, Germany). In order to distinguish different orientation directions, two kinds of cylindrical samples were machined to $\Phi 6\times 20$ mm (unmagnetized state), one with axial direction parallel to orientating direction (parallel direction, $\|$) and the other with axial direction perpendicular to orientating direction (vertical direction, $\perp$). The linear CTE (α_l), the difference of $\mathrm{d}l/l_0$ between two directions $\Delta(\mathrm{d}l/l_0)$ and the slope of $\Delta(\mathrm{d}l/l_0)$ segment k was obtained by the thermal strain ($\mathrm{d}l/l_0$) curve as follows:

$$\alpha_l=\frac{\mathrm{d}l}{l_0\times \mathrm{d}T}, \tag{1}$$
$$\Delta(\mathrm{d}l/l_0)=(\mathrm{d}l/l_0)_{\|}-(\mathrm{d}l/l_0)_{\perp}, \tag{2}$$
$$k=\Delta(\mathrm{d}l/l_0)(@T_c)/(T_c-T_0), \tag{3}$$

where l is the length of the specimen at temperature T, and l_0 is the length at starting temperature (T = 20 °C). The Curie temperature (T_c) of sintered magnets was determined corresponding to the minimum of CTE curves.[21]

3. Results and discussion

3.1. Effects of Co content

The demagnetization curves of Co0, Co6, and Co12 magnets are shown in Fig. 1(a). By comparing the magnetic properties of the magnets with different Co contents, the coercivity of Co12 magnet (H_{cj} = 13.74 kOe, 1 Oe = 79.5775 A·m^{-1}) is lower than Co0 (H_{cj} = 21.08 kOe) and the remanence B_r almost constant. One of the main reasons is that the anisotropy field (H_A) of $R_2Co_{14}B$ compound is about 30% lower than the $R_2Fe_{14}B$ compound.[22] Figure 1(b) shows the remanence temperature coefficient α_{B_r} (25 °C–100 °C) and the Curie temperature T_c for three. By comparing α_{B_r} and T_c of S-NdFeB with different Co contents, α_{B_r} and T_c are improved gradually with the increase of Co content. As the Co content x increases from 0 wt% to 12 wt%, T_c increases almost linearly by more than 137 °C, and the remanence temperature coefficient improves from −0.112%/°C to −0.075%/°C. Overall, with the increase of Co content, the temperature stability of S-NdFeB has been significantly improved and H_{cj} decreases.

Figure 2(a) presents x-ray diffraction patterns of powder samples prepared from Co0, Co6, and Co12 magnets, revealing that the main phase remains as tetragonal $Nd_2Fe_{14}B$-type phase as the Co content increases, consistent with prior literature.[23–25] Notably, the peaks shift to higher angles with increasing Co content, indicating the incorporation of Co atoms into the main phase and a reduction in the lattice parameters. Figure 2(b) shows the crystal lattice structure of the $Nd_2Fe_{14}B$ compound. Figure 2(c) reveals a monotonic decrease in both the a and c parameters with increasing Co content (the parameters were determined by Rietveld method using the GSAS-2). Cause of that Co atoms tend to selectively substitute for Fe at the $8j_1$ crystallographic site, while the exchange interaction between the $8j_1$ & $8j_2$ sites is negative. As Co has a smaller magnetic moment (6.4 μ_B) than Fe (6.7 μ_B), the substitution of Co for Fe reduces the negative exchange interaction and enhances the exchange interaction between 3d atoms, leading to a decrease in lattice parameters.[20] Consequently, the Curie temperature of the magnet increases while the spontaneous magnetostriction phenomenon weakens.[19]

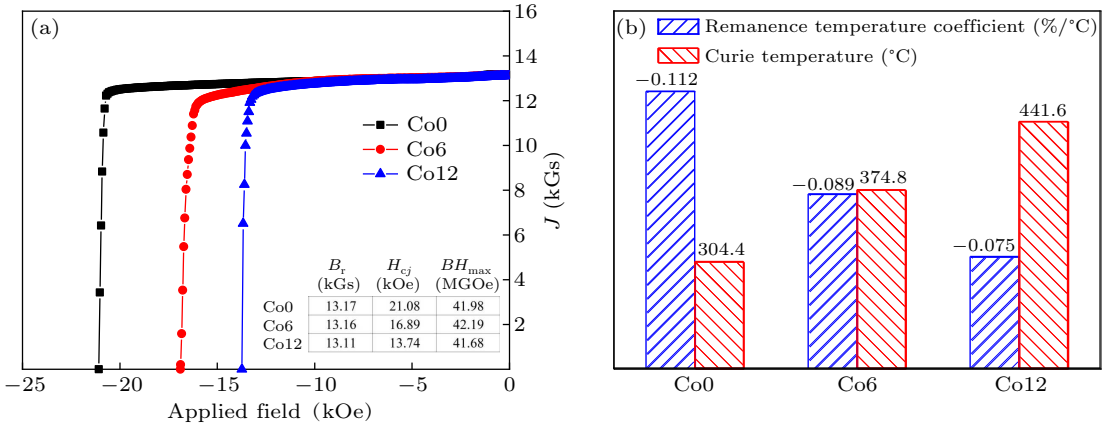


Fig. 1. Demagnetization curves (at 25 °C) and (b) remanence temperature coefficient (25 °C–100 °C) and Curie temperature for Co0, Co6, and Co12 magnets. The unit 1 Gs = 10^{-4} T.

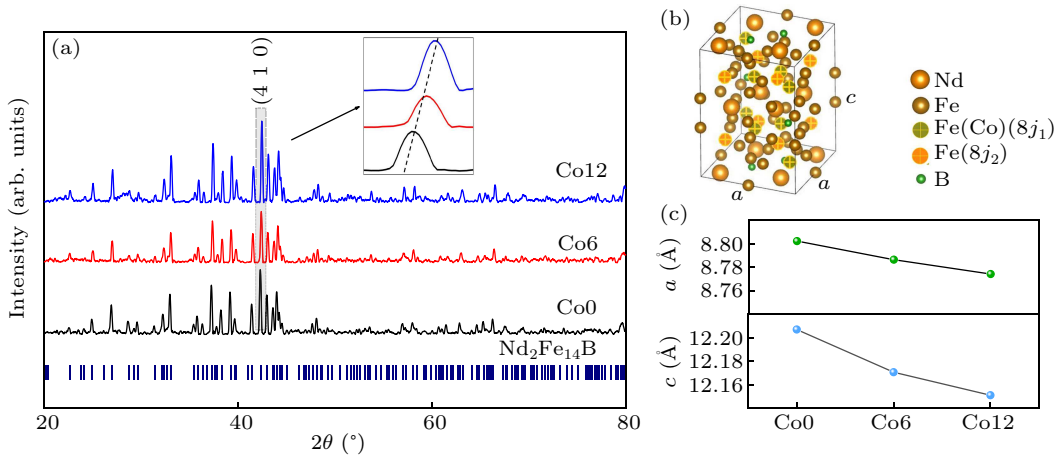


Fig. 2. XRD diffraction patterns of Co0, Co6, and Co12 magnets, (b) crystal lattice structure of $Nd_2(Fe,Co)_{14}B$ compound, (c) lattice parameters of Co0, Co6, and Co12 magnets.

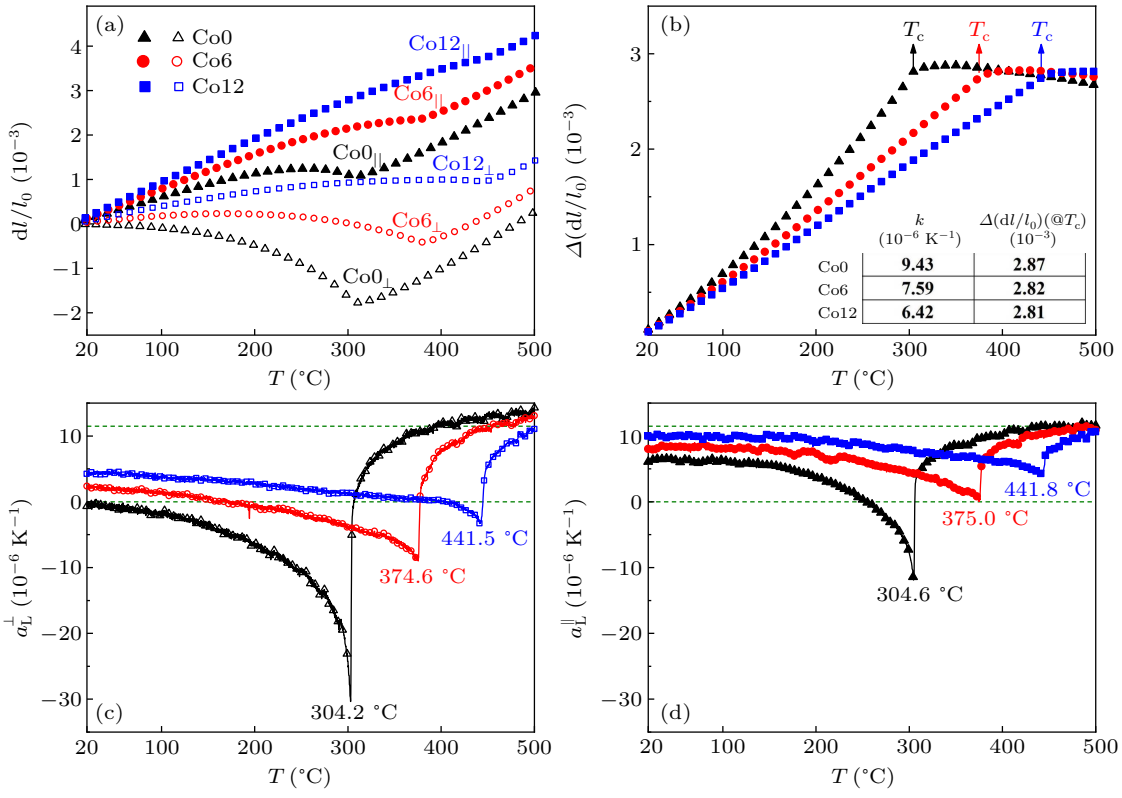


Fig. 3. Temperature dependence of (a) dl/l_0, (b) $\Delta(dl/l_0)$, (c) $\alpha_l^{\perp}$, (d) $\alpha_l^{||}$ for Co0, Co6, and Co12 magnets.

Figure 3(a) compares the temperature dependence of relative elongation for three (thermal strain curves, in two directions). To further analyze the thermal expansion behavior, the curves of $\alpha_l^{\perp}$ and $\alpha_l^{\parallel}$ are shown in Figs. 3(c) and 3(d), respectively (α_l is the first derivate of dl/l_0). It is found that the α_l curves are divided into two segments by T_c. Below T_c, there is a clear trend that both $\alpha_l^{\perp}$ and $\alpha_l^{\parallel}$ increase with Co content. For Co0, the value of $\alpha_l^{\perp}$ is less than zero throughout, showing a great NTE. While for Co6, the curve of $\alpha_l^{\perp}$ crosses the zero line, showing a variation from PTE to NTE. And for Co12, the value of $\alpha_l^{\perp}$ is larger than former two, showing PTE in the almost entire range. These findings may help us to development S-NdFeB with zero linear thermal expansion (with Co content of 6 wt%–12 wt%). However, contrary to the great difference of CTE below T_c, the curves of both $\alpha_l^{\perp}$ and $\alpha_l^{\parallel}$ with different Co contents approach to the dotted line ($\alpha_l \approx 11.5\times10^{-6}$ K^{-1}) with the increase of temperature far above T_c. Although due to the narrow temperature range in this study, compare to the data in high temperature regions from other studies,[18,19] it can be inferred that thermal expansion behavior of S-NdFeB tends to be isotropic with the increase of temperature in a certain range above T_c.

Below T_c, the increase of Co content not only makes CTE larger, but also makes the anisotropy of the thermal expansion weaker. As shown in Fig. 2(b), $\Delta(dl/l_0)$ between two directions increases approximately linearly below T_c, while remaining almost at the same level above T_c. After linear fitting, the slopes of the segments for three magnets below T_c, k are $k(\text{Co0}) = 9.43\times10^{-6}$ K^{-1}, $k(\text{Co6}) = 7.59\times10^{-6}$ K^{-1}, and $k(\text{Co12}) = 6.42\times10^{-6}$ K^{-1}, respectively. In the same range of temperature, larger k means greater anisotropy of thermal expansion. For example, from 20 °C to 200 °C, $\Delta(dl/l_0)$ between two directions of Co12 is 31.9% smaller than Co0. Furthermore, $\Delta(dl/l_0)$ at T_c is used to approximate the maximum of $\Delta(dl/l_0)$. With a negligible difference, the values of $\Delta(dl/l_0)(@T_c)$ are 2.87×10^{-3}, 2.82×10^{-3}, and 2.81×10^{-3} for Co0, Co6, and Co12, respectively.

As shown in Table 1, the average linear CTE (20 °C–100 °C) of Co12 (S-NdFeB with 12-wt% Co) is close to the soft magnetic alloys, which is more favorable for assembling and welding than ordinary S-NdFeB (Co0). Meanwhile, the reduced anisotropy of thermal expansion also represents less likely to crack when preparing rings. The magnetic properties of Co12 magnet are the remanence $B_r = 13.11$ kGs (1 Gs $= 10^{-4}$ T), the coercivity $H_{cj} = 13.74$ kOe, the maximum magnetic energy product $(BH)_{max} = 41.68$ MGOe, and a high Curie temperature $T_c = 441.8$ °C.

Accordingly, below T_c, with the increase of Co content, both $\alpha_l^{\perp}$ and $\alpha_l^{\parallel}$ increase and the anisotropy of thermal expansion decreases, and $\Delta(dl/l_0)(@T_c)$ is almost constant; compared to the large variation below T_c, Co content has little effect on the thermal expansion behavior far above T_c. The substitution of Co for Fe will enhance the 3d atomic exchange interaction, leading to a reduction in spontaneous magnetostriction, which directly affects the thermal expansion of the R_2(Fe, Co)$_{14}$B lattice. Practically, in order to compensate for the lower H_{cj} due to the substitution of Co for Fe, heavy rare earth (HRE) as Dy and Tb can be added. However, HRE is bad for $(BH)_{max}$ and the effect to CTE needs further study.

Table 1. Average linear CTE (20 °C–100 °C) for normal S-NdFeB, soft magnetic alloys, and magnet samples in this study.

Materials	$\alpha_l^{\parallel}$ (10^{-6} K^{-1})	$\alpha_l^{\perp}$ (10^{-6} K^{-1})	$\Delta\alpha_l(=\alpha_l^{\parallel}-\alpha_l^{\perp})$ (10^{-6} K^{-1})
Normal S-NdFeB	4 ~ 9	−2 ~ 0	6 ~ 9[5]
Carbon steel	10.6 ~ 12.2[6]		–
Nickel–iron alloys	6.81 ~ 13.0[7]		–
Iron–cobalt alloys	9.2 ~ 10.7[8]		–
Iron–chromium alloys	9.9[9]		–
Iron–aluminum alloys	12.0 ~ 13.3[10]		–
Co	6.31	1.02	7.33
Co6	8.27	1.22	7.05
Co12	9.90	4.17	5.73
0 A	3.79	3.67	0.12
30 A	8.12	1.92	6.2
60 A	8.33	1.52	6.81
90 A	8.40	1.43	6.97

3.2. Effects of orientation

As figure 4(a) shows, remanence B_r and squareness H_k/H_{cj} are greatly affected by orientation. By comparing the oriented 90-A magnet with non-oriented 0-A magnet, remanence B_r increases from 6.55 kGs to 12.77 kGs and squareness H_k/H_{cj} increases from 27% to 96%. Figure 4(b) shows the XRD pattern of the magnets with different orientations. The ratio of the relative intensities between (006) and (105), $(I_{(006)}/I_{(105)})$, is often used to represent the orientation degree for S-NdFeB. In general, with the increase of current, the magnetic field increases, so the magnetic powders get better aligned, as confirmed by the increase of $I_{(006)}/I_{(105)}$. To enable a direct comparison of the grain alignment, EBSD was used to observe the surface perpendicular to orientation direction of the 0-A and 90-A samples. Figures 4(c) and 4(d) show the inverse pole figure (IPF) mapping of 0 A and 90 A, in which the black part is the grain boundary phase and the other part is $R_2Fe_{14}B$-type phase (grains whose c-axis is parallel to the orientating direction will be shown in red). For the oriented 90-A magnet, the value of $I_{(006)}/I_{(105)}$ is 1.43 in XRD pattern and the majority of the grains is red in IPF mapping, showing a good orientation. However, for the non-oriented 0-A magnet, it shows a lack of strong diffraction peaks on the (006) and (105) crystal planes in XRD pattern, and grains do not tend to be a certain color in IPF mapping, indicating that the c axis of the grains in 0 A is randomly distributed. Combined with the above analysis, the degree of orientation for oriented magnet increases gradually with the increase of the current producing the magnetic field, and there is a large difference with non-oriented magnet.

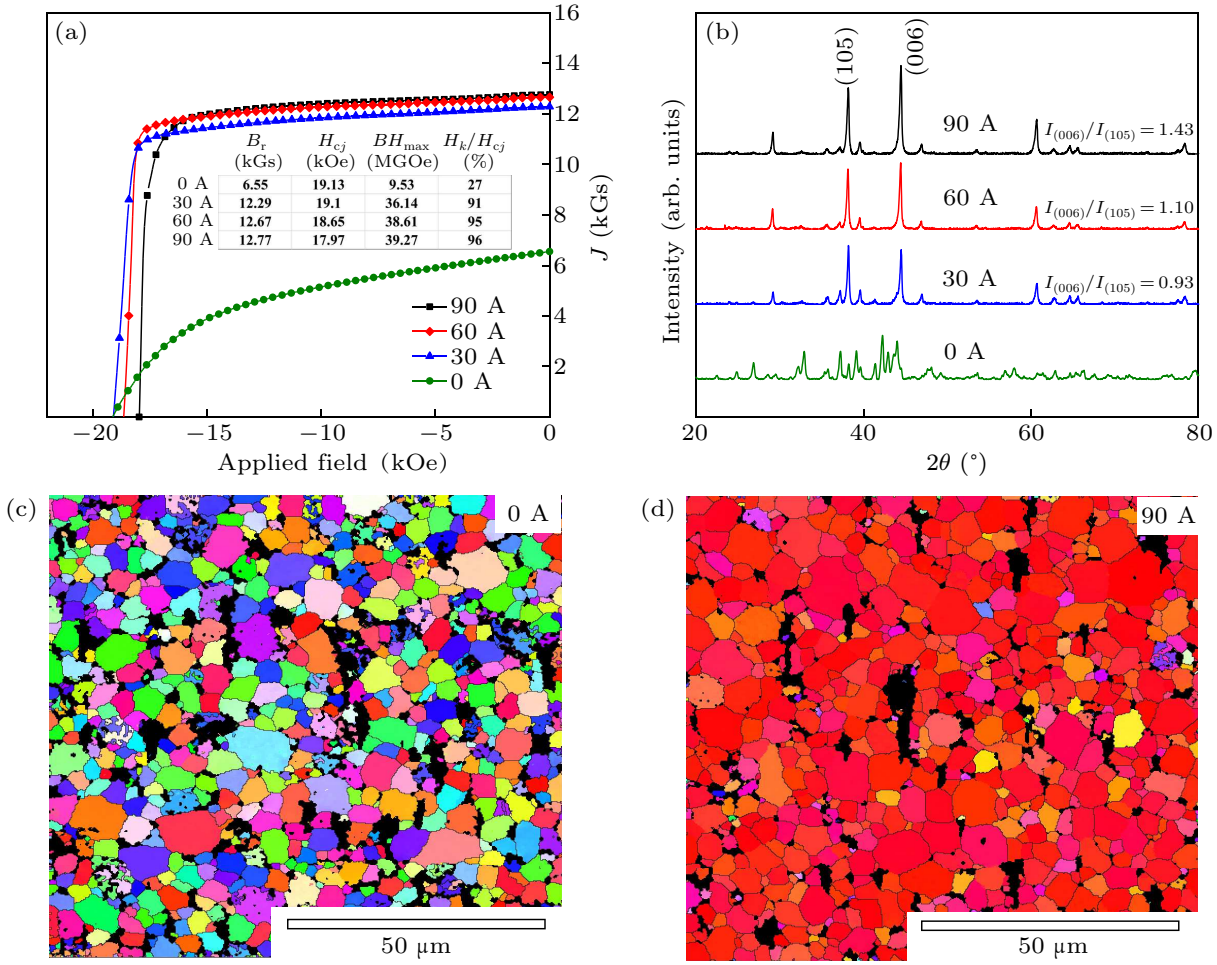


Fig. 4. Representation of orientation (a) demagnetization curves, (b) XRD patterns for 0 A, 30 A, 60 A, 90 A (at 25 °C), (c) IPF mapping of 0 A, (d) IPF mapping of 90 A.

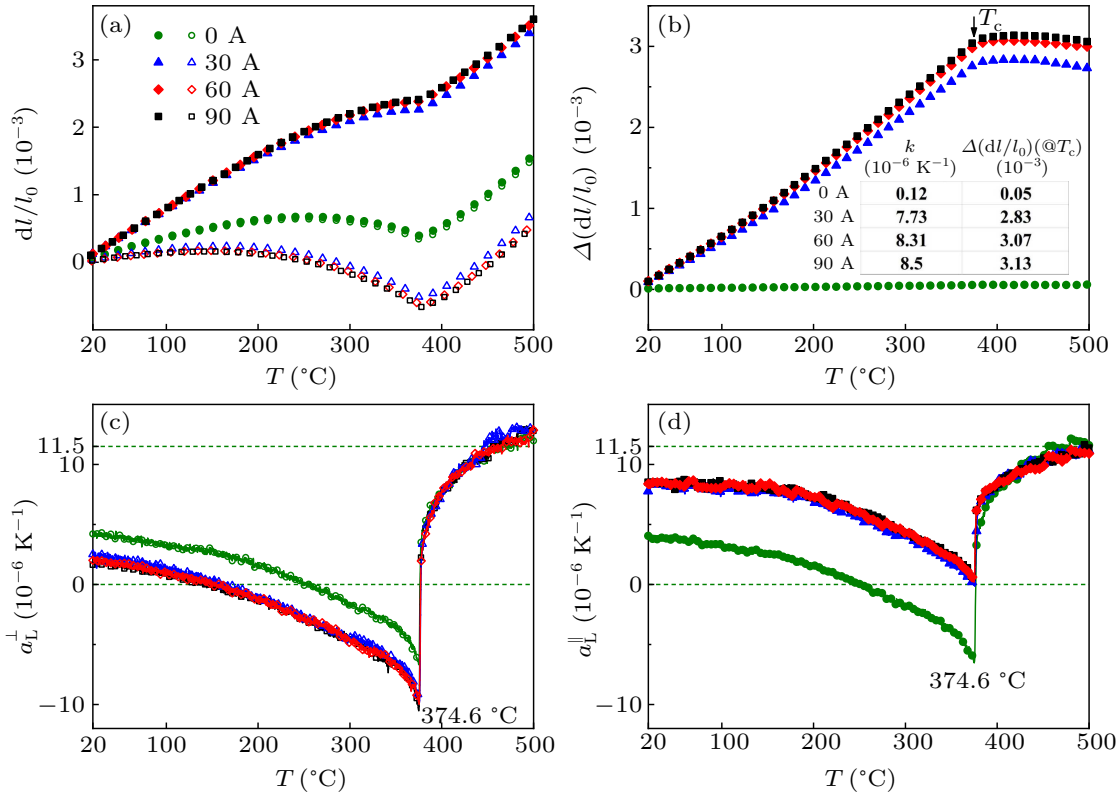


Fig. 5. Temperature dependence of (a) dl/l_0, (b) $\Delta(dl/l_0)$, (c) $\alpha_1^{\perp}$, (d) $\alpha_1^{\parallel}$ for 0-A, 30-A, 60-A, and 90-A magnets.

Figure 5 shows the thermal expansion characteristics of 0-A, 30-A, 60-A, and 90-A magnets, and the difference is mainly reflected in the anisotropy. As shown in Fig. 5(a), the curves on parallel and vertical direction of 0 A almost coincide together, while the value of $\Delta(\mathrm{d}l/l_0)$ in Fig. 5(b) is also almost 0. That means the thermal expansion of 0 A can be considered to be isotropic. The curves of $\Delta(\mathrm{d}l/l_0)$ are shown in Fig. 5(b), each of which increases approximately linearly below T_c and almost remains at the same level above T_c, but $\Delta(\mathrm{d}l/l_0)(@T_c)$ have significant inconsistency:

$$\Delta(\mathrm{d}l/l_0)(@T_c)(30\ \mathrm{A}) = 2.83\times10^{-3},$$
$$\Delta(\mathrm{d}l/l_0)(@T_c)(60\ \mathrm{A}) = 3.07\times10^{-3},$$
$$\Delta(\mathrm{d}l/l_0)(@T_c)(90\ \mathrm{A}) = 3.13\times10^{-3}.$$

Since T_c is the same but $\Delta(\mathrm{d}l/l_0)(@T_c)$ is different, the slopes of the segments below T_c representing anisotropy also differ:

$$k(30\ \mathrm{A}) = 7.73\times10^{-6}\ \mathrm{K}^{-1},\quad k(60\ \mathrm{A}) = 8.31\times10^{-6}\ \mathrm{K}^{-1},$$
$$k(90\ \mathrm{A}) = 8.50\times10^{-6}\ \mathrm{K}^{-1}.$$

It is worth noticing that, as listed in Eq. (3), the k-value change is caused by different ways, with the Co content mainly changing T_c, while the orientation mainly changing $\Delta(\mathrm{d}l/l_0)(@T_c)$. It can be speculated that, due to the anisotropy of the thermal expansion between incompletely aligned grains will cancel each other out, the thermal expansion behavior of completely oriented magnet will be close to single-phase 2:14:1 compound. Spontaneous magnetostriction produced by the exchange coupling between magnetic atoms is the root cause of anomalous thermal expansion for $R_2Fe_{14}B$ compounds. However, for S-NdFeB with complex microstructure, there are many factors affecting the thermal expansion behavior. In this study, Co content and orientation were found to significantly change the thermal expansion behavior of S-NdFeB. These results have important implications for developing S-NdFeB with controllable CTE.

4. Conclusion

In this study, we observed that the thermal expansion behavior of S-NdFeB magnets can be regulated through Co content and orientation. As the Co content increased from 0 wt% to 12 wt%, the linear average $\alpha_1^{\perp}$ (20 °C–100 °C) changes from $-1.02\times10^{-6}\ \mathrm{K}^{-1}$ to $4.17\times10^{-6}\ \mathrm{K}^{-1}$. This indicates that regulating the Co content can develop S-NdFeB with linear ZTE (a-axis). As illustrated in Fig. 6, Co12, with $\alpha_1^{\parallel} = 9.90\times10^{-6}\ \mathrm{K}^{-1}$, is better suited for assembly with soft magnetic alloys when compared to the original S-NdFeB. In addition, it is worth noting that both Co content and orientation influence the anisotropy of the thermal expansion, although the expression and underlying mechanisms are different. The substitution of Co for Fe affects the lattice of main phase, while the orientation affects arrangement of grains. However, the limitation lies in the fact is that the inevitable reduce of magnetic properties by above two ways. Therefore, further investigation into the joint influence of HRE & Co to CTE and magnetic properties is strongly recommended.

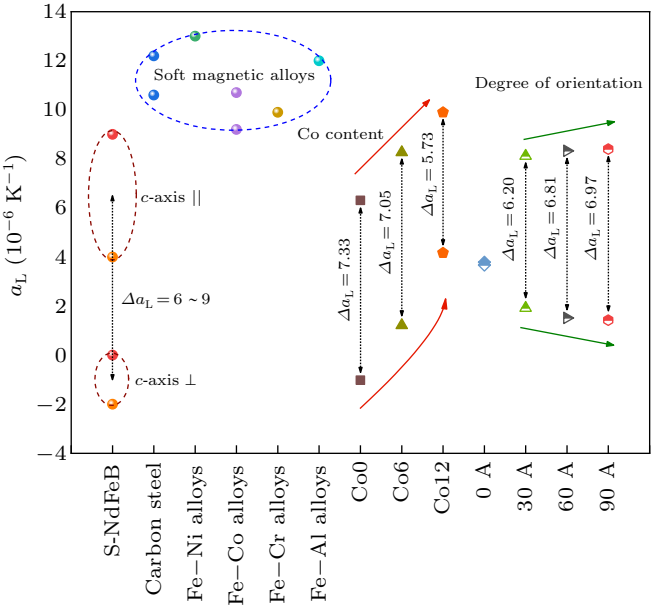


Fig. 6. Average linear CTE (20 °C–100 °C) for normal S-NdFeB, soft magnetic alloys and magnet samples in this study.

Acknowledgments

Project supported by the National Key Research and Development Program of China (Grant No. 2021YFB3502900) and the National Natural Science Foundation of China (Grant No. 51871063), the Key Technology Research and Development Program of Shandong Province, China (Grant No. 2019JZZY020210), and the Major Projects in Inner Mongolia Autonomous Region, China.

References

[1] Sagawa M, Fujimura S, Togawa N, Yamamoto H and Matsuura Y 1984 *J. Appl. Phys.* **55** 2083
[2] Sagawa M, Fujimura S, Yamato H, *et al.* 1984 *IEEE Trans. Magn.* **20** 1584
[3] Wang X C, Yue M, Zhang D T, Liu W Q and Zhu M G 2020 *Rare Metals* **39** 1145
[4] Wang X, Zhao Z R, Liu F, Liu Y L, Wang G F, Zhu M G and Zhang X F 2020 *Rare Metals* **39** 36
[5] GB/T 13560-2017. Sintered neodymium iron boron permanent magnets.
[6] Cheng DX 2017 *Handbook of mechanical design*, 6th edn. (Chemical Industry Press) p. 479 (in Chinese)
[7] GB/T 32286.1-2015 Soft magnetic alloys-Part 1: Nickel-iron alloys
[8] GB/T 14986.3-2018 Soft magnetic alloys-Part 3: Iron-cobalt alloys
[9] GB/T 14986.4-2018 Soft magnetic alloys-Part 4: Iron-chromium alloys
[10] GB/T 14986.5-2018 Soft magnetic alloys-Part 5: Iron-aluminum alloys
[11] Luo C, Qiu X, Wang H, *et al.* 2021 *Journal of Manufacturing Processes.* **64** 323

[12] Sun T, Zhu J and Wang D 1979 *Acta Metallurgica Sinica* **15** 58 (in Chinese)
[13] Ishimoto F, Yamamoto K and Takahashi W 1996 *Journal of the Japan Society of Powder and Powder Metallurgy* **43** 940
[14] Buschow K 1986 *Journal of the Less-Common Metals* **118** 349
[15] Givord D, Li H, Moreau J, *et al.* 1986 *J. Magn. Magn. Mater.* **54–57** 445
[16] Yang N, Dennis K, Mccallum R, *et al.* 2005 *J. Magn. Magn. Mater.* **295** 65
[17] Fujii H, Nagata H, Uwatoko Y, *et al.* 1987 *J. Magn. Magn. Mater.* **70** 331
[18] Teplykh A E, Chukalkin Y, Lee S, Bogdanov S G, Kudrevatykh N V, Rosenfeld E V, Skryabin Yu N, Choi Y, Andreev A V and Pirogov A N 2013 *J. Alloys Compd.* **581** 423
[19] Andreev A V 1990 *Journal of the Less Common Metals.* **162** 33
[20] Qiao Y, Song Y, Xu M, *et al.* 2019 *Inorganic Chemistry Frontiers.* **6** 3225
[21] Gao W, Wang S, Sun M, *et al.* 2020 *Journal of the Chinese Society of Rare Earth* **38** 460 (in Chinese)
[22] Herbst J 1991 *Rev. Modern Phys.* **63** 819
[23] Matsuura Y, Hirosawa S, Yamamoto H, *et al.* 1985 *Appl. Phys. Lett.* **46** 308
[24] Herbst J and Yelon W 1987 *J. Appl. Phys.* **60** 4224
[25] Popov A, Kolodkin D, Gaviko V, *et al.* 2017 *Physics of Metals and Metallography* **118** 935